



# Analysis of properties of the 19 February 2018 volcanic eruption of Mount Sinabung in S5P/TROPOMI and Himawari-8 satellite data

Adrianus de Laat<sup>1</sup>, Margarita Vazquez-Navarro<sup>2,a</sup>, Nicolas Theys<sup>3</sup>, and Piet Stammes<sup>1</sup>

<sup>1</sup>KNMI, De Bilt, 3731 GK, the Netherlands

<sup>2</sup>DLR, Oberpfaffenhofen, 82234 Weißling, Germany

<sup>3</sup>Royal Belgian Institute for Space Aeronomy (BIRA-IASB), Brussels, 1180, Belgium

<sup>a</sup>currently at: EUMETSAT, Darmstadt, Germany

**Correspondence:** Adrianus de Laat (laatdej@knmi.nl)

Received: 4 July 2019 – Discussion started: 2 August 2019

Revised: 27 March 2020 – Accepted: 31 March 2020 – Published: 4 May 2020

**Abstract.** This study presents an analysis of TROPOMI cloud heights as a proxy for volcanic plume heights in the presence of absorbing aerosols and sulfur dioxide for the 19 February 2018 eruption plume of the Sinabung volcano on Sumatra, Indonesia.

Comparison with CALIPSO satellite data shows that all three TROPOMI cloud height data products based on oxygen absorption which are considered here (FRESCO, ROCINN, O22CLD) provide volcanic ash cloud heights comparable to heights measured by CALIPSO for optically thick volcanic ash clouds. FRESCO and ROCINN heights are very similar, with the only differences for FRESCO cloud top heights above 14 km altitude. O22CLD cloud top heights unsurprisingly fall below those of FRESCO and ROCINN, as the O22CLD retrieval is less sensitive to cloud top heights above 10 km altitude. For optically thin volcanic ash clouds, i.e., when Earth's surface or clouds at lower altitudes shine through the volcanic ash cloud, retrieved heights fall below the volcanic ash cloud heights derived from CALIPSO data.

Evaluation of corresponding Himawari-8 geostationary infrared (IR) brightness temperature differences ( $\Delta BT$ s) – a signature for detection of volcanic ash clouds in geostationary satellite data and widely used as input for quantitative volcanic ash cloud retrievals – reveals that for this particular eruption the  $\Delta BT$  volcanic ash signature changes to a  $\Delta BT$  ice crystal signature for the part of the ash plume reaching the upper troposphere beyond 10 km altitude several hours after the start of the eruption and which TROPOMI clearly characterizes as volcanic ( $SO_2 > 1$  DU – Dobson units – and  $AAI > 4$  – absorbing aerosol index – or, more conserva-

tively,  $SO_2 > 10$ ). The presence of ice in volcanic ash clouds is known to prevent the detection of volcanic ash clouds based on broadband geostationary satellite data. TROPOMI does not suffer from this effect and can provide valuable and accurate information about volcanic ash clouds and ash top heights in cases where commonly used geostationary IR measurements of volcanic ash clouds fail.

## 1 Introduction

Monitoring airborne volcanic ash is of crucial importance for aviation planning, as volcanic ash is an environmental hazard that can cause damage to avionics systems, abrasion of exposed airframe parts, engine damage, and even engine failure (Prata and Rose, 2015). From the early 1980s onwards there have been several well-documented damaging encounters of (jet) aircraft with volcanic ash clouds. Since then, aviation authorities have set up working groups and task forces to develop guidelines, procedures, and rules on what to do in case of known or predicted volcanic ash (i.e., ICAO, 2012). The advance of satellite remote-sensing techniques in the early 2000s allowed for real-time global monitoring of volcanic eruptions and airborne volcanic ash and sulfur dioxide ( $SO_2$ ), like the Support to Aviation Control Service – SACS (<http://sacs.aeronomie.be>, last access: 24 April 2020; Brenot et al., 2014) – or the NOAA/CIMSS Volcanic Cloud Monitoring platform (<https://volcano.ssec.wisc.edu/>, last access: 24 April 2020). Nevertheless, in 2010, an eruption of the Icelandic volcano Eyjafjallajökull resulted in the closure of

most of the European airspace, stranding more than 8.5 million people and profoundly affecting commerce (Alexander, 2013). The total economic damage was estimated at USD 2.2 billion (Oxford Economics, 2010). In the aftermath of the 2010 eruption of Eyjafjallajökull, aviation authorities were quick to realize that aviation guidelines for volcanic ash avoidance were too strict. Since then, guidelines have been updated (ICAO, 2012), allowing for more flexibility for aircraft to maneuver around volcanic ash clouds and giving airlines more responsibility. Furthermore, it was also recommended to further develop global real-time volcanic eruption and services monitoring volcanic ash clouds. Ongoing programs by ICAO and WMO continue to work on improving volcanic ash cloud satellite data products that can be used for real-time monitoring of volcanic eruptions and volcanic ash clouds as well as for tactical and strategic flight planning (ICAO, 2012; WMO, 2015, 2017).

However, despite the clear need for constant monitoring of volcanic eruptions and volcanic ash clouds, and despite the availability of a wide variety of satellite remote-sensing data products to meet that particular need, a centralized facility to access and analyze all available remote-sensing data on volcanic eruptions and volcanic ash clouds is still lacking. This strongly hampers integration of that information into aviation operations. As a consequence, volcanic eruptions continue to pose a larger-than-necessary risk for aviation.

In order to fill this information gap, the European Union funded the EUNADICS-AV project by the European Union's Horizon 2020 research program for "Societal challenges – smart, green and integrated transport". The main objective of EUNADICS-AV is "to close the significant gap in European-wide data and information availability during airborne hazards". Volcanic ash clouds are one of those airborne hazards. An important aspect of EUNADICS-AV is to verify how well various satellite instrument are capable of monitoring volcanic eruptions and volcanic ash clouds and how to integrate various satellite data products aboard a variety of satellites. This requires integrated analyses of volcanic ash clouds with the current suite of satellites and remote-sensing data.

For more than a decade, satellite instruments such as SCIAMACHY, OMI, GOME-2, OMPS, AIRS, and IASI have been used to monitor volcanic eruptions in support of aviation. Measurements of SO<sub>2</sub> and the absorbing aerosol index (AAI) are currently provided in near-real time (within 3 h after the satellite spectral measurements) to the aviation community via the SACS web portal, which builds on the TEMIS project, that in 2003 provided the first web-based service that allowed browsing and downloading atmospheric satellite data products, also funded by the ESA.

On 13 October 2017, the ESA successfully launched the TROPOMI instrument as the single payload of the ESA's S5P satellite (Veefkind et al., 2012). TROPOMI is a grating spectrometer that measures Earth-reflected radiances in the ultraviolet (UV), visible, near-infrared (NIR), and short-wave infrared (SWIR) parts of the spectrum, building on the

legacy provided by the satellite instruments OMI and SCIAMACHY. Already a few weeks after launch, TROPOMI started to provide promising high-spatial-resolution measurements (down to 3.5 km × 7 km) of SO<sub>2</sub>, the AAI, and cloud heights from various retrieval algorithms (FRESCO, O22CLD, ROCINN).

Compared to its predecessors, TROPOMI provides measurements with a better signal-to-noise ratio and much better spatial resolution (factor 10 or more, depending on the satellite that it is compared with). This allows for a much better and more detailed characterization of volcanic ash and SO<sub>2</sub> plumes. Furthermore, due to a better spatial resolution and better instrumental signal-to-noise ratio, TROPOMI is expected to provide improved height retrievals of volcanic ash clouds and volcanic SO<sub>2</sub>, important for parameter monitoring purposes (WMO, 2015).

On 19 February 2018, at 08:53 local time, the Indonesian volcano Mount Sinabung on Sumatra generated a dark grey plume with a high volume of ash that quickly rose to an estimated 15–17 km a.s.l., according to the Darwin Volcanic Ash Advisory Centre (VAAC). Ash plumes were identified in satellite images, recorded by webcams and smartphones, and widely shared on social media, also because of the time of the eruption (early morning) and the clear skies at that time. The event was possibly the largest since the beginning of the current episode of unrest at Sinabung, which started in September 2013 (<https://volcano.si.edu/volcano.cfm?vn=261080>, last access: 1 February 2019; Eruptive History).

Mount Sinabung is located in Karo Regency, North Sumatra Province (03°10' N, 98°23.5' E), with a height of 2460 m a.s.l. (Hendrasto et al., 2012; Primulyana et al., 2017; Global Volcanism Program, 2013). The stratovolcano had been dormant for more than 1200 years before it became active again in 2010, and especially since 2013 small eruptions have occurred regularly.

The 19 February 2018 Sinabung eruption provides one of the first possibilities to study the quality of TROPOMI data for volcanic cloud monitoring, also because there was a fortunate overpass of the CALIOP instrument on the CALIPSO satellite. CALIPSO was part of the A-train constellation, which consists of several Earth-observing satellites that closely follow one another, crossing the Equator in an ascending (northbound) direction at about 13:30 local solar time, within seconds to minutes of each other along the same or a very similar orbital "track". The TROPOMI Equator-crossing time is comparable to those of satellites in the A-train constellation. Note that after an orbital maneuver in September 2018, CALIPSO has not been a part of the A-train constellation.

In this paper, we evaluate satellite measurements of the 19 February 2018 Sinabung eruption, with a particular focus on determining volcanic ash cloud heights combining TROPOMI AAI data with TROPOMI cloud height data. We also characterize the volcanic eruption plume in TROPOMI data as well as compare TROPOMI data with geostation-

ary Himawari-8 satellite IR data that are widely used for volcanic ash cloud detection. TROPOMI-based volcanic ash cloud heights are also compared with measurements from the CALIPSO satellite overpass.

## 2 Data

### 2.1 TROPOMI AAI

The AAI is a well-established data product that has been produced for several different satellite instruments spanning a period of more than 30 years. The AAI was first calculated as a correction for the presence of aerosols in column ozone measurements made by the TOMS instruments (Herman et al., 1997; Torres et al., 1998) because it was observed that ozone values were too high in typical regions of aerosol emission and transport. The AAI is based on spectral contrast in the ultraviolet spectral range for a given wavelength pair, where the difference between the observed reflectance and the modeled clear-sky reflectance results in a residual value. When this residual is positive, it indicates the presence of UV-absorbing aerosols, like dust, smoke, or volcanic ash. Clouds yield near-zero residual values, and negative residual values can be indicative of the presence of non-absorbing aerosols (e.g., sulfate), as shown by sensitivity studies of the AAI (e.g., de Graaf et al., 2005; Penning de Vries et al., 2009). Unlike satellite-based aerosol optical thickness measurements, the AAI can also be calculated in the presence of clouds so that daily global coverage is possible. This is ideal for tracking the evolution of episodic aerosol plumes from dust outbreaks, volcanic eruptions, and biomass burning. For this study, we use the TROPOMI AAI data for the wavelength pair 340–380 nm. For more details about the TROPOMI AAI retrieval algorithm, see Stein-Zweers (2016).

### 2.2 TROPOMI SO<sub>2</sub>

Since the late 1970s, a large number of UV-visible satellite instruments have been used for monitoring anthropogenic and volcanic SO<sub>2</sub> emissions. In some cases, operational SO<sub>2</sub> retrieval streams have also been developed, aiming to deliver SO<sub>2</sub> vertical column densities (VCDs) in near real-time (NRT), i.e., typically with a delay of less than 3 h.

The TROPOMI SO<sub>2</sub> retrieval algorithm is based on the DOAS technique (BIRA, 2016; Theys et al., 2017, 2019). In brief, the log ratio of the observed UV-visible spectrum, of radiation backscattered from the atmosphere, and an observed reference spectrum (solar or earthshine spectrum) are used to derive a slant column density (SCD), which represents the SO<sub>2</sub> concentration integrated along the mean light path through the atmosphere. This is done by fitting absorption cross sections of SO<sub>2</sub> to the measured reflectance in a given spectral interval. In a second step, SCDs are corrected for possible biases. Finally, the SCDs are converted into ver-

tical columns by means of air mass factors (AMFs) obtained from radiative transfer calculations, accounting for the viewing geometry, clouds, surface properties, total ozone, and SO<sub>2</sub> vertical profile shapes. The TROPOMI SO<sub>2</sub> data product provides four different SO<sub>2</sub> VCDs for different SO<sub>2</sub> vertical profile shapes, since they are not known at the time of the measurement. For this paper, we use the standard SO<sub>2</sub> VCD data product.

### 2.3 TROPOMI cloud information

TROPOMI provides information about cloud properties by use of oxygen absorption in either the O<sub>2</sub> A-band around 760 nm or the O<sub>2</sub>–O<sub>2</sub> band around 477 nm (Veeffkind et al., 2016). In this study, we use the TROPOMI operational ROCINN cloud height (Loyola et al., 2018; Cloud as Reflecting Boundaries – or CRB – model) and FRESCO cloud height (Wang et al., 2008, 2012), both based on the O<sub>2</sub> A-band and on offline cloud height from the O22CLD algorithm based on the O<sub>2</sub>–O<sub>2</sub> band (Veeffkind et al., 2016). Note that TROPOMI operational cloud fractions are derived from the OCRA algorithm (Loyola et al., 2018). Both the FRESCO cloud height and the O<sub>2</sub>–O<sub>2</sub> cloud height are based on a Lambertian cloud model. Therefore, the retrieved cloud height is the cloud mid-level rather than the cloud top (Wang et al., 2008; Sneep et al., 2008). Note that because the current TROPOMI surface albedo databases – which rely on OMI data – are not fully representative for the TROPOMI spatial resolution and/or wavelengths, this results in inaccurate or unrealistic cloud retrievals which are flagged as missing data. It is expected that in the coming years a surface albedo database will be developed based on the TROPOMI measurements itself, which should solve these retrieval artifacts.

### 2.4 Himawari-8 AHI

The Advanced Himawari-8 Imager (AHI) is a geostationary satellite imager with 16 broadband spectral channels from the visible to IR portion of the electromagnetic spectrum between 0.46 and 13.3 μm. The sub-satellite spatial resolution of AHI is 1 km for all but one VIS channel and 2 km for IR channels. The Himawari-8 AHI is a multipurpose imager that provides full-disk scans of Earth every 10 min from a geostationary orbit at 140.7° E. The imagery can be used for a variety of applications, including general environmental monitoring (e.g., cloud-tracked winds) and numerical weather prediction (Bessho et al., 2016). For the detection of volcanic ash clouds, results from an ad hoc version of the VADUGS algorithm are used (Graf et al., 2015). The VADUGS algorithm is a neural network based on a large number of radiative transfer simulations of geostationary IR brightness temperatures and retrieves the column mass loading (kg m<sup>-2</sup>) and the top altitude of volcanic ash clouds. VADUGS was initially developed for SEVIRI/Meteosat Second Generation (MSG); it has been adapted to Himawari-8 for the purpose

of this paper. VADUGS uses the 10.8–12.0  $\mu\text{m}$  channel  $\Delta\text{BT}$  (brightness temperature difference) for geostationary IR volcanic ash cloud retrieval algorithms. The use of this particular  $\Delta\text{BT}$  is common practice (Prata, 1989), with negative  $\Delta\text{BT}$  potentially indicating volcanic ash and positive  $\Delta\text{BT}$ s indicative of the presence of liquid water or ice content (Pavolonis et al., 2006).

## 2.5 CALIOP

The CALIOP lidar aboard the CALIPSO platform delivers global cloud and aerosol information. The vertical resolution of atmospheric profiles is high, at 30–300 m, but the horizontal sampling is poor, as the satellite is in a low-altitude Earth orbit, with a 16 d repeated cycle, and the horizontal resolution is only 330 m to 5 km (Winker et al., 2007, 2009). In this study, we use 532 nm total attenuated backscatter (TAB) data from one CALIPSO orbit (data version 3.40) in a qualitative approach, i.e., detection of cloud and aerosol layers and their heights. The TAB signal strength is color-coded such that blues correspond to molecular scattering and weak aerosol scattering and aerosols generally show up as yellow–red–orange. Stronger cloud signals are plotted in grey scales, while weaker cloud returns are similar in strength to strong aerosol returns and coded in yellows and reds. The TAB is sensitive to atmospheric particles: both water and ice droplets as well as various types of aerosols.

## 3 Results

### 3.1 Brief description of the spatiotemporal evolution of the volcanic ash cloud

The analysis of Himawari-8 AHI IR brightness temperatures and IR-based volcanic ash cloud heights from CIMSS (Supplement Fig. S1) shows that the 19 February 2018 Sinabung eruption consisted of two distinct components. The initial eruption quickly reached the upper tropical troposphere (14–16 km altitude), after which the volcanic ash cloud was transported in a north–northwesterly direction. These heights are consistent with results from the recently introduced new TROPOMI  $\text{SO}_2$  height data product (Hedelt et al., 2019). Approximately 2 h after the start of the eruption the satellite data show lower-altitude volcanic ash cloud  $\Delta\text{BT}$  signatures (up to 6–8 km altitude) emerging from under the high-altitude volcanic ash cloud at both the northwestern and southeastern end of the high-altitude volcanic ash cloud. As these lower-altitude plumes also move more or less in opposite direction, they more likely reflect remnants of surface pyroclastic flows and/or the eruption column collapse that are also seen in the time-lapse webcam video footage on the internet ([https://youtu.be/v45J5BO\\_ge0](https://youtu.be/v45J5BO_ge0), last access: 24 April 2020).

### 3.2 TROPOMI

Figure 1a shows the TROPOMI FRESKO cloud height and ROCINN cloud pressure, along with the TROPOMI AAI, and the AAI = 0 contour and the  $\text{SO}_2=10$  Dobson unit (DU) contour, with TROPOMI measurements within the figure area made at approximately 06:25 UTC, 4.5 h after the start of the eruption. By then, the volcanic plume had dispersed over an area with an approximate diameter of 200 km, while some parts of the volcanic ash cloud sufficiently thinned so that cumulus clouds lower down in the atmosphere could be identified in VIIRS imagery (see Fig. S2; note that TROPOMI flies in a so-called loose formation with VIIRS, with a temporal separation between both of less than 5 min). The AAI and  $\text{SO}_2$  contours agree well with the cloud structure associated with the volcanic plume, indicating that there was not a spatial separation between volcanic ash and  $\text{SO}_2$ , which is known to sometimes happen in volcanic eruptions (Cooke et al., 2014; Moxnes et al., 2014; Prata et al., 2017). Guided by the AAI and  $\text{SO}_2$  contour lines, the ash cloud can be identified in the FRESKO cloud height and ROCINN cloud pressure – in particular for cloud tops above 10 km – as well as in the FRESKO and O22CLD scene pressures (Fig. 1b), but not in the FRESKO cloud fraction (Fig. 1b), probably because of light absorption by ash. Comparing the cloud height with the VIIRS reflectances (Fig. S2), the volcanic plume altitudes occur where the ash cloud is sufficiently optically thick to not show the underlying surface and clouds.

All cloud height products show the same spatial structure, with the highest clouds in the northern half of the ash plume. The FRESKO and ROCINN cloud heights both consistently indicate cloud heights of 10 km or higher, the O22CLD cloud heights also reach 10 km but for fewer pixels, and in general FRESKO and ROCINN cloud heights are higher than the O22CLD cloud heights (Fig. 1b). The O22CLD data product is based on absorption of the  $\text{O}_2\text{--O}_2$  complex and is less sensitive to high-altitude clouds, as concentrations of the  $\text{O}_2\text{--O}_2$  complex decrease strongly above approximately 10 km altitude (Acarreta et al., 2004). The O22CLD algorithm is therefore computationally limited to maximum cloud top pressures of 150 hPa ( $\sim 13$  km). FRESKO and ROCINN are based on absorption of  $\text{O}_2$ , whose concentrations decrease much slower above 10 km altitude. The FRESKO and ROCINN cloud heights can therefore be used up to approximately 17 km altitude ( $\sim 100$  hPa; Wang et al., 2012). The lower cloud height of O22CLD vs. FRESKO and ROCINN is thus most likely due to the lower sensitivity of O22CLD for high clouds. Differences between FRESKO and ROCINN for the volcanic plume appear less striking, most notably the lack of saturated pixels in ROCINN (greys in FRESKO), which is possible due to the neural network filling in the gaps with nearby cloud information or interpolating between cloud pixels. However, it appears that FRESKO cloud heights are higher for the northern half of the ash plume. FRESKO cloud

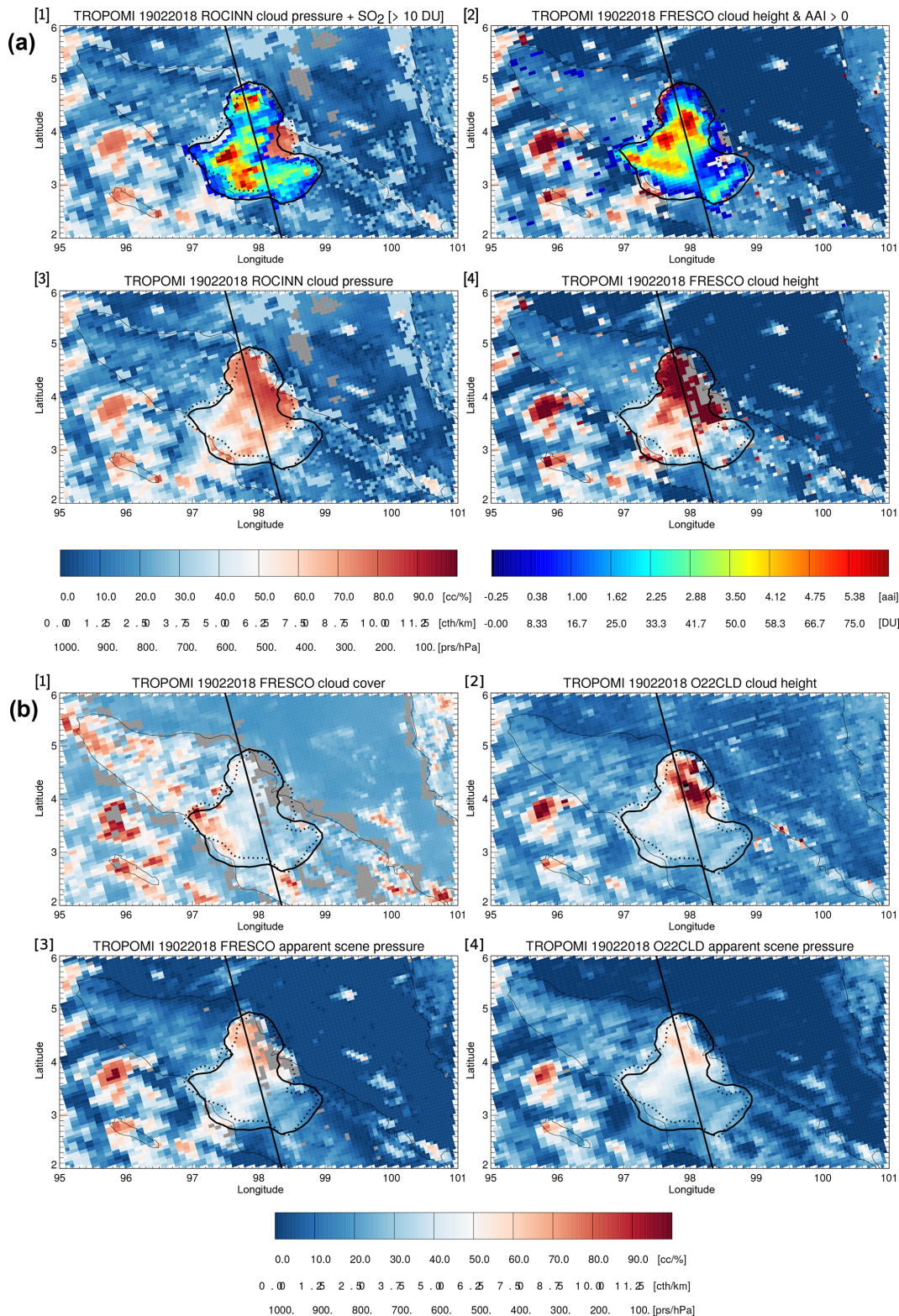


**Figure 1.** (a) TROPOMI cloud pressure (ROCINN; **a1** and **3**) and TROPOMI FRESKO cloud heights (**a2** and **4**). TROPOMI SO<sub>2</sub> (**a1**) and the AAI (**a2**) for the overpass of the 19 February 2018 Sinabung eruption. The straight line denotes the path of the CALIPSO overpass, the solid-line shape denotes the outline of > 10 DU SO<sub>2</sub> columns, and the dotted-line shape denotes the AAI > 0 value. Note that for FRESKO and ROCINN cloud heights certain pixels are greyed out (“no data”), related to yet-unresolved retrieval artifacts. (b) As in (a) but for TROPOMI FRESKO cloud cover (**b1**), O22CLD cloud height (**b2**), FRESKO apparent scene pressure (**b3**), and O22CLD apparent scene pressure (**b4**). cc is cloud cover, cth is cloud top height, and prs is cloud pressure and scene pressure.

heights exceed 12.5 km, which is approximately 200 hPa; ROCINN cloud pressure does not appear to exceed 200 hPa.

### 3.3 CALIOP

Although the 19 February 2018 Sinabung eruption was small in spatial extent and rather short-lived, by mere accident there was a perfect overpass with the CALIOP instrument in the A-train constellation (see Fig. 1). The CALIOP track goes straight through the core of the volcanic ash cloud and across the north–south gradient in cloud tops.

Figure 2 shows the CALIOP backscatter signal at 532 nm overlaid with the TROPOMI FRESCO cloud heights, which are color-coded according to the corresponding AAI values. The CALIOP overpass time of this area is between 07:09:56 and 07:11:26 UTC, and the TROPOMI overpass time is between 06:24:23 and 06:26:00 UTC, a time difference of approximately 45 min. The CALIOP data clearly show not only a cloud–ash layer around 15 km altitude but also two cloud–ash structures extending from the ground up to approximately 10 km altitude, with an increase in height going from south to north. There is also a layer detected in CALIPSO at 18 km around 3° N, which likely is also volcanic, as the Himawari-8  $\Delta BT$  does not provide any indication of other high clouds, while there are negative  $\Delta BT$ s near the CALIPSO track at 3° N, indicative of the presence of volcanic ash.

There is a good agreement between the location of enhanced TROPOMI AAI values, FRESCO cloud height, and the altitude of high backscatter signal in the CALIOP data. The maximum cloud height in FRESCO agrees with the maximum backscatter height in CALIOP between 4 and 5° latitude. Between 3 and 4° latitude, the agreement is poor, as the FRESCO cloud height falls right in between the CALIOP backscatter data between 13 and 18 km altitude and those close to the surface. The CALIOP data also suggest that backscatter signals between 3 and 4° latitude are weaker than between 4 and 5° latitude, which might indicate less dense ash or clouds. For a semi-transparent cloud or ash plume, it could be expected that FRESCO cloud heights are lower than the actual height of the cloud or ash plume due the presence of bright clouds nearer to the surface. Note that CALIOP's own feature mask does not identify hardly any of these backscatter signals as aerosol (for CALIOP v4.10 an occasional cloud pixel is flagged as aerosol; see Hedelt et al., 2019): the high-altitude structures are flagged as regular clouds, and the below-cloud structure as “totally attenuated”, even though clearly the attenuation is not complete. The lack of aerosol masking in the feature mask most likely is related to liquid water or ice contaminating the volcanic ash (Hedelt et al., 2019).

Figure 3 shows the corresponding cloud heights from the O22CLD and ROCINN algorithms. The ROCINN cloud height is very similar to the FRESCO cloud height ( $R^2 = 0.98$  for FRESCO cloud heights between 0.5 and 14 km

regardless of corresponding AAI value). The only difference occurs for FRESCO cloud heights > 14 km, where the ROCINN cloud height appears to be nearly constant around 12 km or 200 hPa. For the O22CLD data the maximum heights are on average lower than the FRESCO and ROCINN cloud heights. The lower cloud height of the O22CLD product is likely related to the reduced sensitivity of O22CLD for clouds above approximately 10 km altitude. Nevertheless, all products clearly indicate volcanic cloud heights of 10 km and higher, with the largest heights between 4 and 5° latitude, consistent with the CALIOP observation that backscatter signals between 3 and 4° latitude are weaker than between 4 and 5° latitude.

Although the CALIOP overpass is perfect in space, the time difference between TROPOMI and CALIOP of approximately 45 min is not insignificant. It is therefore unlikely that TROPOMI and CALIOP ash layers and structures exactly match. The flow direction of the volcanic ash cloud was northwards, which means that CALIOP should also be displaced north compared to TROPOMI. A rough estimate of northward cloud motion based on the geostationary satellite data indicates that the displacement may be approximately  $0.5^\circ \text{ h}^{-1}$ , which makes it not unreasonable to assume that some of the discrepancies between TROPOMI and CALIOP could also be related to the differences in observation time. Furthermore, volcanic eruption plumes have their own dynamics, with for example pyroclastic flows near the surface which appear to travel partly in the opposite direction of the background flow. The eruption dynamics may thus have additional effects on the ash plume displacement, for which time series of the complete three-dimensional view of the eruption plume would be preferred. The current available satellite data only provide a two-dimensional view of the eruption plume from above (geostationary, polar orbiting), with information about changes over time in case of the geostationary satellites and with some, but limited, information about cloud and aerosol height. CALIOP measurements only provide one two-dimensional cross section through the eruption plume, without any information about changes over time.

### 3.4 Himawari-8

The temporal evolution of the ash plume was further investigated using Himawari-8 geostationary IR observations. Figure 4 shows the Himawari-8 10.8–12.0  $\mu\text{m}$  channel ( $\Delta BT$ ) as observed between 02:30 and 07:30 UTC in hourly intervals, including the TROPOMI  $\text{SO}_2$  and AAI contours shown in Fig. 1.

During the first few hours (02:30–03:30 UTC), the ash plume is clearly visible both in the  $\Delta BT$ s (reddish colors) and cloud heights (whites). At 03:30 UTC, two distinct clouds emerge with fairly negative  $\Delta BT$ s: one associated also with a high cloud height (white cloud colors) and another one further south with much lower cloud heights, likely

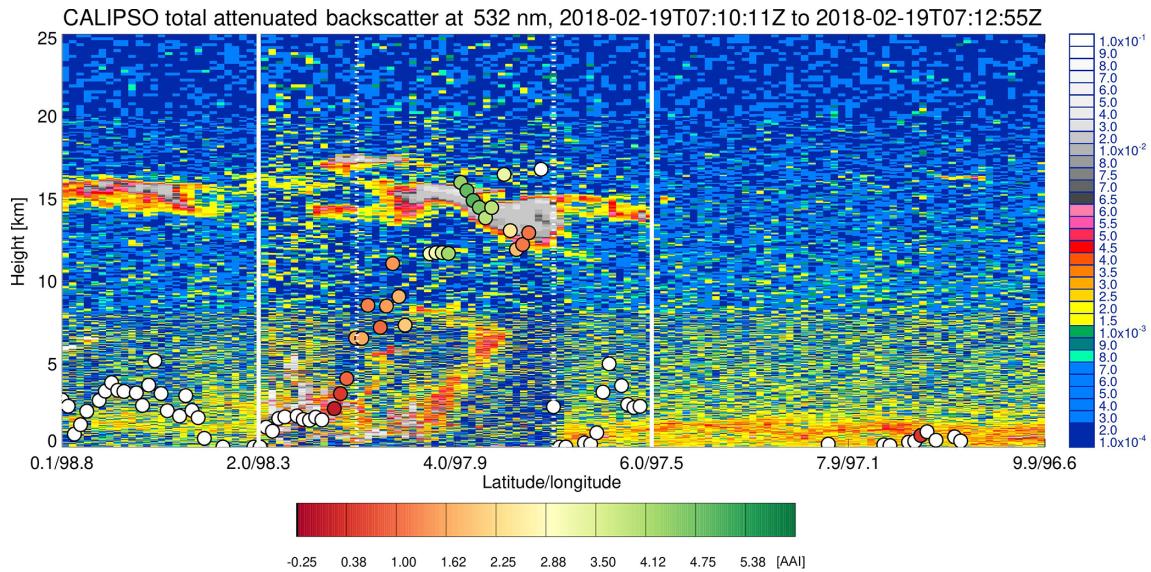


**Figure 2.** CALIOP total attenuated backscatter profile for the Sinabung eruption on 19 February 2018 along the track indicated in Fig. 1. The circles denote the TROPOMI FRESCO cloud heights, color-coded according to the TROPOMI AAI values as in Fig. 1. White dots indicate AAI values < 0.

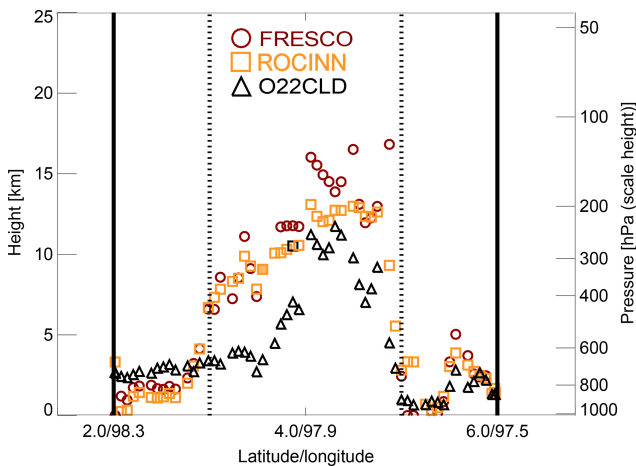


**Figure 3.** TROPOMI cloud heights from the FRESCO, ROCINN and O22CLD algorithms. The solid vertical lines denote the 2 and 6° N latitudes; the dotted vertical lines denote the 3 and 5° latitudes. The FRESCO data are identical to the FRESCO data shown Fig. 2.

low-altitude outflow or pyroclastic flows (blue cloud colors). From 04:30 UTC onwards, a third region becomes visible, with high cloud heights and large positive  $\Delta BT$ s (purple), indicative of high ice clouds, which continues to grow and expand northward.

Figure 5 shows a comparison of TROPOMI AAI and  $SO_2$  data with regridded Himawari-8  $\Delta BT$ s (Fig. 5a). When focusing on AAI and  $SO_2$  values, it appears that larger  $\Delta BT$  values occur for smaller AAI values (< 2) and  $SO_2$  columns (< 10 DU). The largest positive  $\Delta BT$ s are associated with optically thicker and less transparent water and ice clouds (see

also VIIRS imagery in the SI and comparison of TROPOMI with CALIPSO). The lack of larger AAI and  $SO_2$  values for larger positive  $\Delta BT$  values therefore may reflect some kind of shielding of the volcanic ash and  $SO_2$  by the iced upper levels of the volcanic ash cloud.  $SO_2$  may have been converted into sulfate as the  $SO_2$  depletion rate (*e*-folding time), which, although uncertain, has been estimated to be as small as 5–30 min (Oppenheimer et al., 1998; McGonigle et al., 2004), scavenged by ice (Rose et al., 2000) or via ice nucleation of volcanic ash particles (Durant et al., 2008). For negative  $\Delta BT$ s – indicative of volcanic ash clouds – we also find little evidence of a distinctive relation between either the AAI or  $SO_2$  with  $\Delta BT$ s. This may similarly reflect a shielding effect, as the largest aerosol concentrations are not associated with the largest possible  $\Delta BT$ s (e.g., Prata and Prata, 2012; Pavolonis et al., 2006).

The emergence of an IR ice–water cloud signature within the volcanic ash cloud is consistent with analysis of available video footage and pictures on social media that show signs of condensation within the ash clouds soon after the start of the eruption. This is indicative of a moist troposphere in this area, which is further supported by the widespread development of (late) afternoon thunderstorms on 19 February throughout Sumatra. The eruption thus caused an increase in high-altitude water vapor, either by moisture contained in the eruption itself or by the rapid vertical motions within the eruption column. The results presented here support the notion that the IR volcanic ash cloud  $\Delta BT$  signature disappears when condensed water vapor or ice forms in a volcanic ash cloud, which is known to significantly hamper IR volcanic

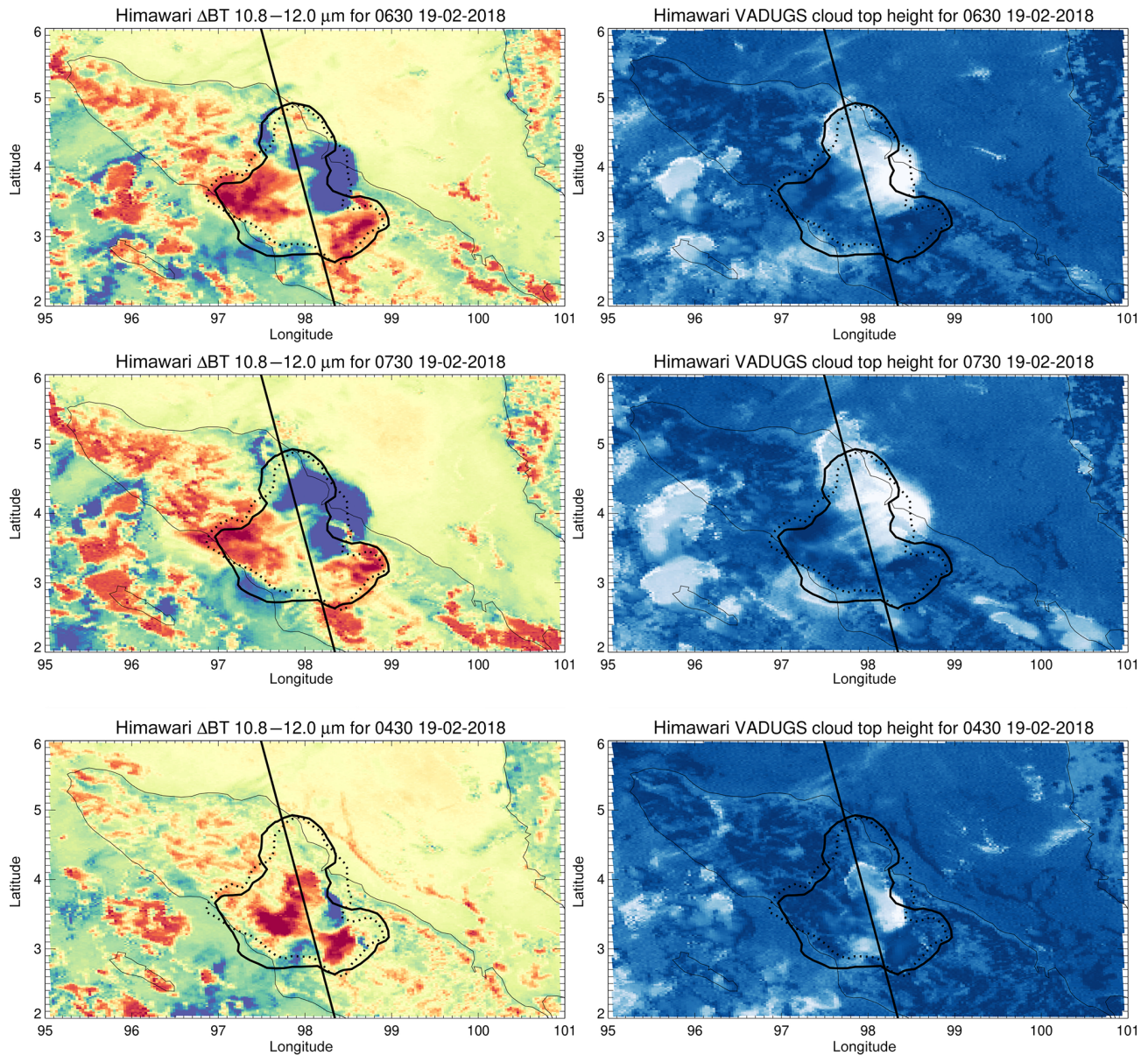


**Figure 4.**

ash cloud retrievals (Francis et al., 2012; Pavolonis et al., 2015a, b; Zhu et al., 2017).

#### 4 Discussion and conclusions

Analysis of measurements from the polar-orbiting TROPOMI satellite – with unprecedented spatial resolution and accuracy – of the volcanic eruption of Mount Sinabung on Sumatra on 19 February 2018 has revealed that the combination of the TROPOMI AAI and TROPOMI SO<sub>2</sub> allows for accurate identification of the volcanic ash cloud location. In addition, under the condition that the ash plume is sufficiently thick so that clouds and the Earth

surface below the ash cloud are not visible, TROPOMI cloud heights also provide accurate information about the volcanic ash cloud heights. The TROPOMI FRESCO and ROCINN cloud heights agree with CALIOP cloud top measurements for optically thick volcanic ash clouds. However, there is a difference between FRESCO and ROCINN for very high FRESCO heights (> 12.5 km or approximately 200 hPa). This might indicate that the ROCINN neural network may not be sufficiently trained on clouds beyond 12 km or 200 hPa. In passing we note that the unprecedented spatial resolution of TROPOMI allows for detection of much smaller eruptions than is currently possible with polar-orbiting satellite instruments like OMPS, GOME-2, and

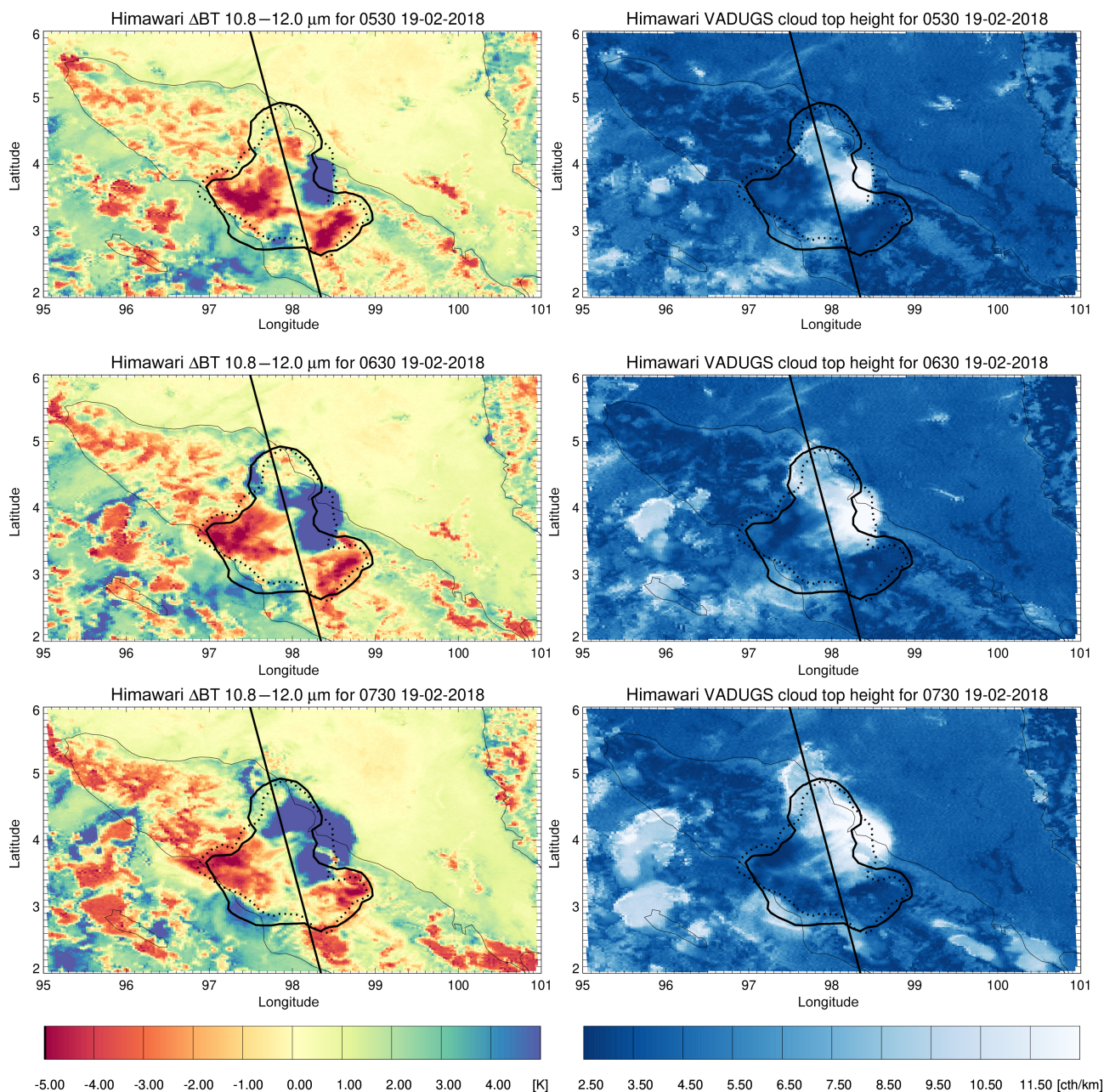


**Figure 4.** Himawari-8 VADUGS cloud heights (right) and 10.8–12.0  $\mu\text{m}$   $\Delta\text{BT}$ s (left) for every hour between 02:30 and 07:30 UTC. The line denotes the CALIPSO overpass track. The solid and dotted contours denote outline of TROPOMI  $> 10 \text{ DU}$   $\text{SO}_2$  columns and TROPOMI  $\text{AAI} > 0$  value, as shown in Fig. 1.

OMI. Also note that it could be argued that it would be better to use the TROPOMI  $\text{SO}_2$  15 km data product, as 15 km is more consistent with the volcanic plume height. However, this 15 km data product assumes a “nice-and-tidy”  $\text{SO}_2$  plume without any contamination, let alone the complexity of a fresh, optically very thick eruption plume and the presence of condensed water, in combination with indications of a shielding effect. Furthermore, the main focus of this paper is ash heights rather than  $\text{SO}_2$ , which is mostly used

as a proxy for a volcanic plume, although investigating the accuracy and precision of satellite  $\text{SO}_2$  VCD observations in fresh volcanic plumes would be valuable, in particular with soon-to-be-launched geostationary hyperspectral satellites.

Comparison with CALIOP aerosol and cloud heights provides clear indications that ash height estimates using cloud heights and AAI values from UV–VIS satellites like TROPOMI may underestimate actual ash heights in case of semi-transparent volcanic ash clouds, especially in the

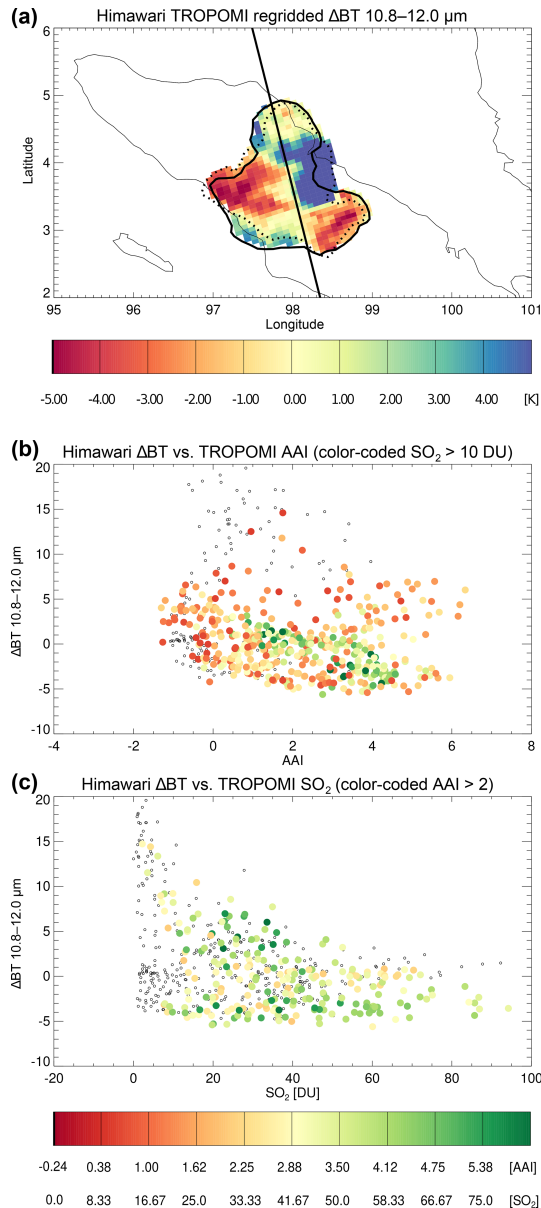


**Figure 5.** (a) Himawari-8  $\Delta BT$ s for 19 February 2018 at 06:30 UTC (see also Fig. 4) regrided to the TROPOMI measurement grid of that day, and correlations between the Himawari-8  $\Delta BT$ s and TROPOMI (b) AAI and (c)  $SO_2$ . The solid and dotted contours denote outline of TROPOMI  $> 10$  DU  $SO_2$  columns and TROPOMI AAI  $> 0$  value, as also shown in Fig. 4 and in Fig. 1. The color-coding of the dots in the AAI scatterplots is indicative of the corresponding  $SO_2$  value ( $> 10$  DU), and the color-coding in the  $SO_2$  scatterplot is indicative of the AAI value (AAI  $> 2$ ); see also the lower color bar. These color-codings were added for qualitatively identifying possible relationships between  $\Delta BT$  and AAI or  $SO_2$  within the volcanic ash cloud.

presence of high concentrations of water vapor and for very high-altitude volcanic ash clouds. For volcanic ash clouds optically thin enough for light to pass through, the TROPOMI cloud heights are a weighted mean of the ash height and heights of other clouds or the surface and are therefore less useful for the purpose of monitoring volcanic ash cloud height. Some discrepancies between TROPOMI and CALIPSO may be related due to misalignment in observation times of both satellite instruments ( $\sim 45$  min). In addition, indications were found of shielding of volcanic ash by this ice and water near the top of the volcanic ash cloud.

There are also clear indications in the geostationary IR data of the formation of water and ice near the top of the volcanic ash cloud. The analysis of geostationary satellite data for this particular case revealed that under conditions of volcanic ash mixed with ice of condensed water, the geostationary IR volcanic ash cloud  $\Delta BT$  signature is lost and geostationary volcanic ash cloud retrievals cannot identify crucial parts of the ash plume. It is worth mentioning that the temporal resolution inherent in the geostationary orbit allows the observation of the onset and evolution of the plume, even in adverse conditions for the IR volcanic ash cloud retrieval algorithm.

Polar-orbiting satellites like TROPOMI thus may be better able to detect volcanic ash when condensed ice and water are present in volcanic plumes, in particular when synergistically combining different satellite data products like the AAI and  $SO_2$ . Furthermore, for the present case study, large negative  $\Delta BT$ s appear not to be a good indicator of large AAI values (or large  $SO_2$  columns). This is not surprising, as highly negative  $\Delta BT$ s do not necessarily indicate large ash optical depth values (e.g., Prata and Prata, 2012; Pavolonis et al., 2006). Our results therefore highlight that there is added value in combining IR  $\Delta BT$  with the UV–VIS AAI and  $SO_2$ . Satellite measurements like those from TROPOMI measurements thus can add significant value to geostationary IR volcanic ash cloud retrievals. Furthermore, in case of sufficiently dense ash, the cloud height data products provide accurate volcanic ash cloud heights, an important piece of information for aviation. For semi-transparent volcanic ash clouds, where the cloud top height retrievals become sensitive to other reflective surfaces below the transparent volcanic ash clouds, detection of accurate volcanic ash cloud heights is limited.

Hence, for AAI values larger than 4, TROPOMI cloud heights can be used for determining aerosol heights, and in case also  $SO_2$  is detected, such measurements should be interpreted as also containing volcanic ash (column values  $> 1$  DU; Theys et al., 2017). For more conservative estimates  $SO_2$  column values  $> 10$  could be considered. This AAI threshold value of 4 may be conservative but ensures that the aerosol layer very likely is opaque, as generally the associated aerosol optical depth will be (very) large (de Graaf et al., 2005). For the combination of UV–VIS cloud heights, the AAI and  $SO_2$  could also be used for other UV–VIS satellites like GOME-2, OMPS, and OMI. These results highlight

the importance of the integrated use of multiple (satellite) data sources for the detection and characterization of volcanic ash clouds, in particular for aviation purposes. This has been recognized by the European Union and is being further developed within the Horizon 2020 project EUNADICS-AV (<http://www.eunadics.eu>, last access: 24 April 2020).

## Appendix A: Glossary

AAI	Absorbing aerosol index
AIRS	Atmospheric infrared sounder
AMF	Air mass factor
AHI	Advanced Himawari-8 Imager
BIRA	Belgian Institute for Space Aeronomy
$\Delta$ BT	Brightness temperature difference
CALIOP	Cloud-Aerosol Lidar with Orthogonal Polarization
CALIPSO	Cloud-Aerosol Lidar and Infrared Pathfinder Satellite Observation
CIMSS	Cooperative Institute for Meteorological Satellite Studies
DOAS	Differential optical absorption spectroscopy
DU	Dobson unit
ESA	European Space Agency
EUNADICS-AV	European Natural Airborne Disaster Information and Coordination System for Aviation
FRESCO	Fast Retrieval Scheme for Clouds from the Oxygen A-band
GOME-2	Global Ozone Monitoring Experiment–2
ICAO	International Civil Aviation Organization
IASI	Infrared atmospheric sounding interferometer
IR	Infrared
NOAA	National Oceanic and Atmospheric Administration
NRT	Near-real time
OCRA	Optical Cloud Recognition Algorithm
OMI	Ozone monitoring instrument
OMPS	Ozone Mapping Profiler Suite
O22CLD	O <sub>2</sub> –O <sub>2</sub> cloud
ROCINN	Retrieval Of Cloud Information using Neural Networks
SACS	Support for Aviation Control Service
SCD	Slant column density
SCIAMACHY	SCanning Imaging Absorption spectromETER for Atmospheric CHartographY
SCOPE	Sustained, Coordinated Processing of Environmental Satellite Data for Nowcasting
SO <sub>2</sub>	Sulfur dioxide
S5P	Sentinel-5 Precursor
TAB	Total attenuated backscatter
TEMIS	Tropospheric Emission Monitoring Internet Service
TOMS	Total Ozone Mapping Spectrometer
TROPOMI	TROPOspheric Monitoring Instrument
UTC	Universal time coordinated
UV	Ultraviolet
VAAC	Volcanic Ash Advisory Centre
VADUGS	Volcanic Ash Detection Utilizing Geostationary Satellites
VCD	Vertical column density
VIS	Visible
VIIRS	Visible Infrared Imaging Radiometer Suite
WMO	World Meteorological Organization

*Data availability.* TROPOMI SO<sub>2</sub>, AAI, ROCINN, and FRESCO data are publicly accessible via <https://s5phub.copernicus.eu/> (ESA, 2018). TROPOMI O<sub>2</sub>CLD data can be made available on request by contacting the lead author or by contacting KNMI. Data were processed by Maarten Sneep (KNMI) and provided on 1 February 2019. CALIOP data are freely available via the ICARE Data and Services Center (<http://www.icare.univ-lille1.fr/>) (Vaughan et al., 2019). HIMAWARI and VADUGS data were processed by Margarita Vazquez Navarro (then at DLR, Germany) and provided on 29 June 2018. Data can be made available on request by contacting the lead author. VIIRS imagery as shown in the Supplement is freely accessible at NASA Worldview <https://worldview.earthdata.nasa.gov/> (last access: 1 February 2019).

*Supplement.* The supplement related to this article is available online at: <https://doi.org/10.5194/nhess-20-1203-2020-supplement>.

*Author contributions.* AdL contributed to the conceptualization, investigation, methodology, visualization, formal analysis, and writing the original draft. MVN, NT, and PS contributed to data curation and reviewing and editing the writing.

*Competing interests.* The authors declare that they have no conflict of interest.

*Special issue statement.* This article is part of the special issue “Analysis and prediction of natural airborne aviation hazards”. It is not associated with a conference.

*Acknowledgements.* The authors thank the two anonymous referees for their thoughtful and valuable comments. This paper is supported by the European Union’s Horizon 2020 research and innovation program under grant agreement no. 723986, project EUNADICS-AV (European Natural Airborne Disaster Information and Coordination System for Aviation).

*Financial support.* This research has been supported by the Horizon 2020 Societal Challenges, Horizon 2020 Transport (EUNADICS-AV (grant no. 723986)).

*Review statement.* This paper was edited by Marcus Hirtl and reviewed by two anonymous referees.

## References

Acarreta, J. R., de Haan, J. F., and Stammes, P.: Cloud pressure retrieval using the O<sub>2</sub>-O<sub>2</sub> absorption band at 477 nm, *J. Geophys. Res.*, 109, D05204, <https://doi.org/10.1029/2003JD003915>, 2004.

Alexander, D.: Volcanic ash in the atmosphere and risks for civil aviation: a study in European crisis management, *Int. J. Disaster. Risk Sc.*, 4, 9–19, <https://doi.org/10.1007/s13753-013-0003-0>, 2013.

Bessho K., Date, K., Hayashi, M., Ikeda, A., Imai, T., Inoue, H., Kumagai, Y., Miyakawa, T., Murata, M., Ohno, T., Okuyama, A., Oyama, R., Sasaki, Y., Shimazu, Y., Shimoji, K., Y. Sumida, Y., Suzuki, M., Taniguchi, H., Tsuchiyama, H., Uesawa, D., Yokota, Y., and Yoshida, R., An introduction to Himawari-8/9 – Japan’s new-generation geostationary meteorological satellites, *J. Meteorol. Soc. Jpn.*, 94, 151–183, <https://doi.org/10.2151/jmsj.2016-009>, 2016.

BIRA: S5P/TROPOMI SO<sub>2</sub> ATBD, S5P-BIRA-L2-400E-ATBD, available at: [http://www.tropomi.eu/sites/default/files/files/S5P-BIRA-L2-ATBD-SO2\\_400E\\_v1.1.0\\_20181005.pdf](http://www.tropomi.eu/sites/default/files/files/S5P-BIRA-L2-ATBD-SO2_400E_v1.1.0_20181005.pdf) (last access: 1 February 2019), 2016.

Brenot, H., Theys, N., Clarisse, L., van Geffen, J., van Gent, J., Van Roozendaal, M., van der A, R., Hurtmans, D., Coheur, P.-F., Clerbaux, C., Valks, P., Hedelt, P., Prata, F., Rason, O., Sievers, K., and Zehner, C.: Support to Aviation Control Service (SACS): an online service for near-real-time satellite monitoring of volcanic plumes, *Nat. Hazards Earth Syst. Sci.*, 14, 1099–1123, <https://doi.org/10.5194/nhess-14-1099-2014>, 2014.

Cooke, M. C., Francis, P. N., Millington, S., Saunders, R., and Witham, C.: Detection of the Grímsvötn 2011 volcanic eruption plumes using infrared satellite measurements. *Atmos. Sci. Lett.*, 15, 321–327, <https://doi.org/10.1002/asl2.506>, 2014.

de Graaf, M., Stammes, P., Torres, O., and Koelemeijer, R. B. A.: Absorbing Aerosol Index: Sensitivity analysis, application to GOME and comparison with TOMS, *J. Geophys. Res.*, 110, D01201, <https://doi.org/10.1029/2004JD005178>, 2005.

Durant, A. J., Shaw, R. A., Rose, W. I., Mi, Y., and Ernst, G. G. J.: Ice nucleation and overseeding of ice in volcanic clouds, *J. Geophys. Res.*, 113, D09206, <https://doi.org/10.1029/2007JD009064>, 2008.

ESA: Sentinel-5P Pre-Operations Data Hub, available at: <https://s5phub.copernicus.eu/dhus> (last access: 1 February 2019), 2018.

Francis, P. N., Cooke, M. C., and Saunders, R. W.: Retrieval of physical properties of volcanic ash using Meteosat: A case study from the 2010 Eyjafjallajökull eruption, *J. Geophys. Res.*, 117, D00U09, <https://doi.org/10.1029/2011JD016788>, 2012.

Graf, K. Kox, S., Schmidl, M., and Gasteiner, J.: the VADUGS algorithm, Volcanic Ash Detection using Geostationary Satellites, presentation at the WMO Intercomparison Workshop, Madison, Wisconsin, United States, 29 June–2 July 2015, available at: [http://cimss.ssec.wisc.edu/meetings/vol\\_ash15/PDFs/20150630/Item2.10\\_20150630\\_WMO\\_Madison\\_Graf.pdf](http://cimss.ssec.wisc.edu/meetings/vol_ash15/PDFs/20150630/Item2.10_20150630_WMO_Madison_Graf.pdf) (last access: 1 February 2019), 2015.

Global Volcanism Program: Mount Sinabung (261080), *Volcanoes of the World*, v4.8.6, edited by: E. Venzke, <https://doi.org/10.5479/si.GVP.VOTW4-2013>, Smithsonian Institution, 2013.

Hedelt, P., Efremenko, D. S., Loyola, D. G., Spurr, R., and Clarisse, L.: Sulfur dioxide layer height retrieval from Sentinel-5 Precursor/TROPOMI using FP\_ILM, *Atmos. Meas. Tech.*, 12, 5503–5517, <https://doi.org/10.5194/amt-12-5503-2019>, 2019.

Hendrasro, M., Surono, A., Budianto, K., Triastuty, H., Haerani, N., Basuki, A., Suparman, Y., Primulyana, S., Prambada, O., Loeqman, A., Indrastuti, N., Andreas, A. S., Rosadi, U., Adi,

- S., Iguchi, M., Ohkura, T., Nakada, S., and Yoshimoto, M.: Evaluation of volcanic activity at Sinabung volcano, after more than 400 years of quiet, *Journal of Disaster Research*, 7, 37–47, <https://doi.org/10.20965/jdr.2012.p0037>, 2012.
- Herman, J. R., Bhartia, P. K., Torres, O., Hsu, C., Seftor, C., and Celarier, E. A.: Global distributions of UV-absorbing aerosols from NIMBUS 7/TOMS data, *J. Geophys. Res.*, 102, 16911–16922, <https://doi.org/10.1029/96JD03680>, 1997.
- ICAO: Flight Safety and Volcanic Ash, ICAO Document 9974, available at: [http://www.icao.int/publications/Documents/9974\\_en.pdf](http://www.icao.int/publications/Documents/9974_en.pdf), (last access: 1 May 2018), 2012.
- Loyola, D. G., Gimeno García, S., Lutz, R., Argyrouli, A., Romahn, F., Spurr, R. J. D., Pedernana, M., Doicu, A., Molina García, V., and Schüssler, O.: The operational cloud retrieval algorithms from TROPOMI on board Sentinel-5 Precursor, *Atmos. Meas. Tech.*, 11, 409–427, <https://doi.org/10.5194/amt-11-409-2018>, 2018.
- McGonigle, A. J. S., Delmelle, P., Oppenheimer, C., Tsanev, V. I., Delfosse, T., Williams-Jones, G., Horton, K., and Mather, T. A.: SO<sub>2</sub> depletion in tropospheric volcanic plumes, *Geophys. Res. Lett.*, 31, L13201, <https://doi.org/10.1029/2004GL019990>, 2004.
- Moxnes, E. D., Kristiansen, N. I., Stohl, A., Clarisse, L., Durant, A., Weber, K., and Vogel, A.: Separation of ash and sulfur dioxide during the 2011 Grímsvötn eruption, *J. Geophys. Res.-Atmos.*, 119, 7477–7501, <https://doi.org/10.1002/2013JD021129>, 2014.
- Oppenheimer, C., Francis, P., and Stix, J.: Depletion rates of sulfur dioxide in tropospheric volcanic plumes, *Geophys. Res. Lett.*, 25, 2671–2674, 1998.
- Oxford Economics: available at: [https://www.tcd.ie/Economics/assets/pdf/SER/2014/elin\\_thora.pdf](https://www.tcd.ie/Economics/assets/pdf/SER/2014/elin_thora.pdf) (last access: 1 February 2019), 2010.
- Pavolonis, M. J., Feltz, W. F., Heidinger, A. K., and Galina, G. M.: A Daytime Complement to the Reverse Absorption Technique for Improved Automated Detection of Volcanic Ash, *J. Atmos. Ocean. Tech.*, 23, 1422–1444, <https://doi.org/10.1175/JTECH1926.1>, 2006.
- Pavolonis, M. J., Sieglaff, J., and Cintineo, J.: Spectrally Enhanced Cloud Objects – A generalized framework for automated detection of volcanic ash and dust clouds using passive satellite measurements: 1. Multispectral analysis, *J. Geophys. Res.-Atmos.*, 120, 7813–7841, <https://doi.org/10.1002/2014JD022968>, 2015a.
- Pavolonis, M. J., Sieglaff, J., and Cintineo, J.: Spectrally Enhanced Cloud Objects – A generalized framework for automated detection of volcanic ash and dust clouds using passive satellite measurements: 2. Cloud object analysis and global application, *J. Geophys. Res.-Atmos.*, 120, 7842–7870, <https://doi.org/10.1002/2014JD022969>, 2015b.
- Penning de Vries, M. J. M., Beirle, S., and Wagner, T.: UV Aerosol Indices from SCIAMACHY: introducing the SCattering Index (SCI), *Atmos. Chem. Phys.*, 9, 9555–9567, <https://doi.org/10.5194/acp-9-9555-2009>, 2009.
- Prata, A. J.: Infrared radiative transfer calculations for volcanic ash clouds, *Geophys. Res. Lett.*, 16, 1293–1296, <https://doi.org/10.1029/GL016i011p01293>, 1989.
- Prata, A. J. and Prata, A. T.: Eyjafjallajökull volcanic ash concentrations determined using Spin Enhanced Visible and Infrared Imager measurements, *J. Geophys. Res.*, 117, D00U23, <https://doi.org/10.1029/2011JD016800>, 2012.
- Prata, A. and Rose, W. I.: Volcanic Ash Hazards and Aviation, Chapter 52 in *The Encyclopedia of Volcanoes*, second edition, edited by: Sigurdsson, H., Houghton, B., McNutt, S. R., Rymer, H., and Stix, J., ISBN 978-0-12-385938-9, 2015.
- Prata, F., Woodhouse, M., Huppert, H. E., Prata, A., Thordarson, T., and Carn, S.: Atmospheric processes affecting the separation of volcanic ash and SO<sub>2</sub> in volcanic eruptions: inferences from the May 2011 Grímsvötn eruption, *Atmos. Chem. Phys.*, 17, 10709–10732, <https://doi.org/10.5194/acp-17-10709-2017>, 2017.
- Primulyana, S., Kern, C., Lerner, A., Saing, U. B., Kunrat, S. L., Alfianti, H., and Marlia, M.: Gas and ash emissions associated with the 2010–present activity of Sinabung Volcano, Indonesia, *J. Volcanol. Geoth. Res.*, 382, 184–196, <https://doi.org/10.1016/j.jvolgeores.2017.11.018>, 2017.
- Rose, W. I., Bluth, G. J. S., and Ernst, G. G. J.: Integrating retrievals of volcanic cloud characteristics from satellite remote sensors: a summary, edited by: Francis, P., Neuberg, J., and Sparks, R. S. J., *Philos. T. R. Soc. A*, 358, 1585–1606, <https://doi.org/10.1098/rsta.2000.0605>, 2000.
- Sneep, M., de Haan, J. F., Stammes, P., Wang, P., Vanbauce, C., Joiner, J., Vasilkov, A. P., and Levelt, P. F.: Three-way comparison between OMI and PARASOL cloud pressure products, *J. Geophys. Res.*, 113, D15S23, <https://doi.org/10.1029/2007JD008694>, 2008.
- Stein-Zweers, D.: TROPOMI ATBD of the UV aerosol index, S5P-KNMI-L2-0008-RP, available at: [http://www.tropomi.eu/sites/default/files/files/S5P-KNMI-L2-0008-RP-TROPOMI\\_ATBD\\_UVAI-1.1.0-20180615\\_signed.pdf](http://www.tropomi.eu/sites/default/files/files/S5P-KNMI-L2-0008-RP-TROPOMI_ATBD_UVAI-1.1.0-20180615_signed.pdf) (last access: 1 February 2019), 2016.
- Theys, N., De Smedt, I., Yu, H., Danckaert, T., van Gent, J., Hörmann, C., Wagner, T., Hedelt, P., Bauer, H., Romahn, F., Pedernana, M., Loyola, D., and Van Roozendaal, M.: Sulfur dioxide retrievals from TROPOMI onboard Sentinel-5 Precursor: algorithm theoretical basis, *Atmos. Meas. Tech.*, 10, 119–153, <https://doi.org/10.5194/amt-10-119-2017>, 2017.
- Theys, N., Hedelt, P., De Smedt, I., Lerot, C., Yu, H., Vlietinck, J., Pedernana, M., Arellano, S., Galle, B., Fernandez, D., Carlito, C. J. M., Barrington, C., Taisne, B., Delgado-Granados, H., Loyola, D., and van Roozendaal, M.: Global monitoring of volcanic SO<sub>2</sub> degassing with unprecedented resolution from TROPOMI onboard Sentinel-5 Precursor, *Nat. Sci. Rep.*, 9, 2643, <https://doi.org/10.1038/s41598-019-39279-y>, 2019.
- Torres, O., Bhartia, P. K., Herman, J. R., Ahmad, Z., and Gleason, J.: Derivation of aerosol properties from satellite measurements of backscattered ultraviolet radiation: Theoretical basis, *J. Geophys. Res.*, 103, 17099–17110, <https://doi.org/10.1029/98JD00900>, 1998.
- Vaughan, M., Pitts, M., Trepte, C., Winker, D., Detweiler, P., Garnier, A., Getzewitch, B., Hunt, W., Lambeth, J., Lee, K.-P., Lucker, P., Murray, T., Rodier, S., Trémas, T., Bazureau, A., and Pelon, J.: CALIPSO data management system data products catalog, document No. PC-SCI-503, Release 4.20, available at: [http://www-calipso.larc.nasa.gov/products/CALIPSO\\_DPC\\_Rev4x20.pdf](http://www-calipso.larc.nasa.gov/products/CALIPSO_DPC_Rev4x20.pdf), last access: 1 February 2019.
- Veefkind, J. P., Aben, I., McMullan, K., Förster, H., de Vriese, J., Otter, G., Claas, J., Eskes, H. J., de Haan, J. F., Kleipool, Q., van Weele, M., Hasekamp, O., Hoogeveen, R., Landgraf, J., Snel, R., Tol, P., Ingmann, P., Voorse, R., Kruizinga, B., Vink, R., Visser, H., and Levelt, P. F.: TROPOMI on the ESA

- Sentinel-5 Precursor: A GMES mission for global observations of the atmospheric composition for climate, air quality and ozone layer applications, *Remote Sens. Environ.*, 120, 70–83, doi:10.1016/j.rse.2011.09.027, 2012.
- Veefkind, J. P., de Haan, J. F., Sneep, M., and Levelt, P. F.: Improvements to the OMI O<sub>2</sub>–O<sub>2</sub> operational cloud algorithm and comparisons with ground-based radar–lidar observations, *Atmos. Meas. Tech.*, 9, 6035–6049, <https://doi.org/10.5194/amt-9-6035-2016>, 2016.
- Wang, P., Stammes, P., van der A, R., Pinardi, G., and van Roozendaal, M.: FRESCO+: an improved O<sub>2</sub> A-band cloud retrieval algorithm for tropospheric trace gas retrievals, *Atmos. Chem. Phys.*, 8, 6565–6576, <https://doi.org/10.5194/acp-8-6565-2008>, 2008.
- Wang, P., Tuinder, O. N. E., Tilstra, L. G., de Graaf, M., and Stammes, P.: Interpretation of FRESCO cloud retrievals in case of absorbing aerosol events, *Atmos. Chem. Phys.*, 12, 9057–9077, <https://doi.org/10.5194/acp-12-9057-2012>, 2012.
- Winker, D. M., Hunt, W. H., and McGill, M. J.: Initial performance assessment of CALIOP, *Geophys. Res. Lett.*, 34, L19803, <https://doi.org/10.1029/2007GL030135>, 2007.
- Winker, D. M., Vaughan, M. A., Omar, A., Hu, Y., Powell, K. A., Liu, Z., Hunt, W. H., and Young, S. A.: Overview of the CALIPSO mission and CALIOP data processing, *J. Atmos. Ocean. Tech.*, 26, 2310–2323, <https://doi.org/10.1175/2009JTECHA1281.1>, 2009.
- WMO: Final Report of the Meeting on the Intercomparison of Satellite-based Volcanic Ash Retrieval Algorithms, Madison WI, USA 29 June–2 July 2015.
- WMO: SCOPE Nowcasting, Volcanic Ash Algorithm Intercomparison – Pilot Project 2, available at: [http://www.wmo.int/pages/prog/sat/meetings/documents/IPET-SUP-3\\_Doc\\_07-01-02\\_SCOPE-NWC-PP2.pdf](http://www.wmo.int/pages/prog/sat/meetings/documents/IPET-SUP-3_Doc_07-01-02_SCOPE-NWC-PP2.pdf) (last access: 1 February 2019), 2017.
- Zhu, L., Li, J., Zhao, Y., Gong, H., and Li, W.: Retrieval of volcanic ash height from satellite-based infrared measurements, *J. Geophys. Res.-Atmos.*, 122, 5364–5379, <https://doi.org/10.1002/2016JD026263>, 2017.